

www.acsami.org Forum Article

Multimaterial Printing for Cephalopod-Inspired Light-Responsive Artificial Chromatophores

Daehoon Han, ** Yueping Wang, ** Chen Yang, and Howon Lee*



Cite This: ACS Appl. Mater. Interfaces 2021, 13, 12735–12745



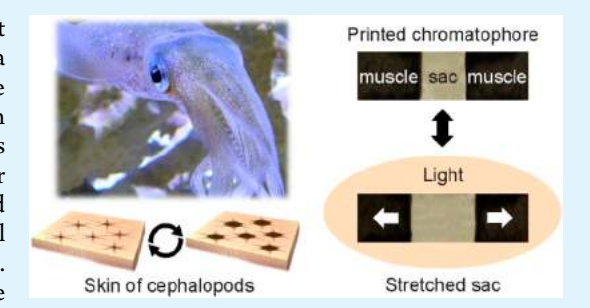
ACCESS I

Metrics & More



Supporting Information

ABSTRACT: Cephalopods use chromatophores distributed on their soft skin to change skin color and its pattern. Each chromatophore consists of a central sac containing pigment granules and radial muscles surrounding the sac. The contraction of the radial muscle causes the central sac to expand in area, making the color of the pigment more visible. With the chromatophores actuating individually, cephalopods can create extremely complex skin color patterns, which they utilize for exquisite functions including camouflage and communication. Inspired by this mechanism, we present an artificial chromatophore that can modulate its color pattern in response to light. Multimaterial projection microstereolithography is used to integrate three functional components including a photoactive hydrogel composite with



polydopamine nanoparticles (PDA-NPs), acrylic acid hydrogel, and poly(ethylene glycol) diacrylate. In order to generate light-driven actuation of the artificial chromatophore, the photothermal effect of the PDA-NPs, light-responsive deformation of the photoactive hydrogel composite, and the produced mechanical stresses are studied. Mechanical properties and interfacial bonding strengths between different materials are also investigated to ensure structural integrity during actuation. We demonstrate pattern modulation of the light-responsive artificial chromatophores (LACs) with the projection of different light patterns. The LAC may suggest a new concept for various engineering applications such as the camouflage interface, biophotonic device, and flexible display.

KEYWORDS: camouflage, cephalopods, light-responsive hydrogels, polydopamine, multimaterial 3D printing

1. INTRODUCTION

Animals such as chameleons and octopuses have developed the incredible ability to reversibly change their skin colors or textures according to their surrounding environment. Among many exquisite camouflage mechanisms in nature, cephalopods, including octopuses, cuttlefishes, and squids, have been extensively studied because of their dramatic and sophisticated camouflage mechanism.¹⁻³ Studies have found that pigmentcontaining and light-reflecting cells that are distributed throughout the cephalopod skin, or chromatophores, play the key role (Figure 1a). A chromatophore consists of a central elastic sac, containing pigment granules, and a series of radial muscles (Figure 1b).4 Contraction of the radial muscles mechanically stretches out the central sac, amplifying the visual expression of the color of the pigment inside the sac. The size of the sac typically increases by three times from approximately 150 to 450 μ m in diameter when the radial muscles contract. Furthermore, a variety of color patterns can be generated on their skin since individual chromatophores contract or expand independently.^{4,5} While the exact mechanism is yet to be uncovered, the distributed cognition and actuation of the active chromatophore network have long been inspiring scientists for its unparalleled potential for novel engineering systems with distributed intelligence.

Color modulation inspired by cephalopods has been demonstrated by various methods including electrokinetics^o and fluorescent patterning with electro-mechanochemically responsive elastomers, mechanochromisms, magnetic nanopigments,⁹ and dielectric elastomers.^{3,10,11} However, they are fundamentally different from the actual camouflage mechanism of cephalopods in that the sensing and actuation were performed separately and the color change was controlled by a central control system, which required bulky and complex auxiliary equipment for applying high voltage, magnetic or electric fields, or mechanical signals. Here, we report a cephalopod-inspired light-responsive artificial chromophore (LAC) that can sense light at the individual unit level and alter its color expression by emulating the cephalopods' camouflage mechanism. The LAC consists of three components: light-responsive muscle, stretchable sac, and rigid frame (Figure 1c). The light-responsive muscle is made of a temperature-responsive hydrogel with embedded polydop-

Special Issue: Novel Stimuli-Responsive Materials for 3D Printing

Received: September 30, 2020 Accepted: December 18, 2020 Published: January 4, 2021





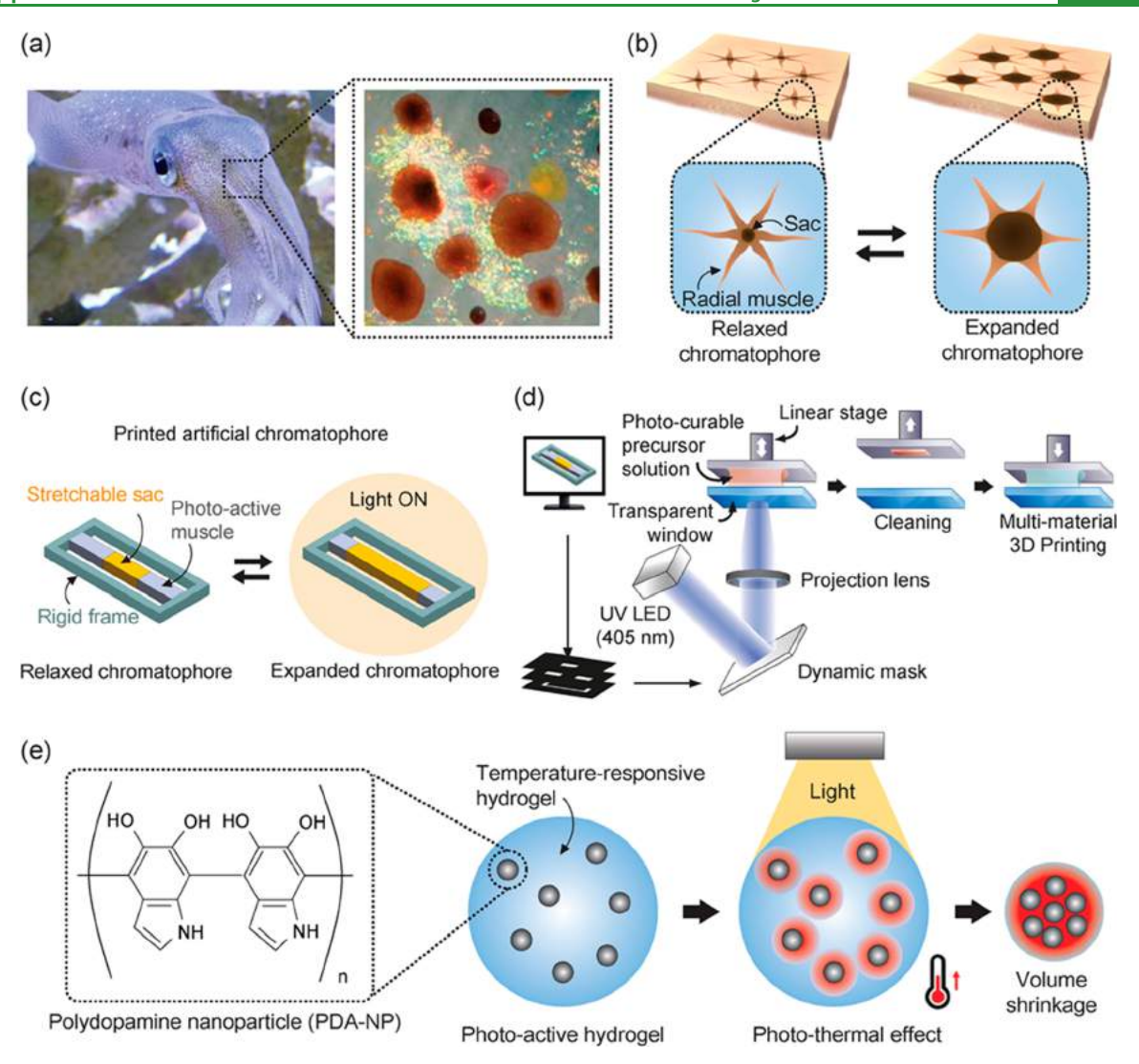


Figure 1. Cephalopod-inspired ligh-responsive artificial chromatophore. (a) Chromatophores in the skin of cephalopods (Reproduced with permission from ref 5. Copyright 2009 The Royal Society). (b) Schematic of actuation of the active chromatophore in the skin. The actual sac can be stretched up to about three times by radial muscles. (c) The printed light-responsive artificial chromatophore consists of three components: light-responsive muscle, stretchable sac, and rigid frame. (d) Schematic illustration of the MM-P μ SL process. (e) Active volume change of the photoactive hydrogel in response to light irradiation. The photoactive hydrogel consists of a temperature-responsive hydrogel and polydopamine nanoparticles (PDA-NPs) as a photothermal agent.

amine nanoparticles (PDA-NPs) as a photothermal agent. Therefore, upon light irradiation, the nanoparticles generate heat to deswell the hydrogel matrix for light-driven contraction, which in turn stretches the sac in the middle. Since these three components have their distinctive roles, we fabricated LACs using a multimaterial three-dimensional (3D) printing technique, multimaterial projection microstereolithography (MM-P\(mu\)SL) (Figure 1d).\(^{12-15}\) We prepared photocurable precursor solutions for the three components and investigated the photothermal effect, light-responsive deformation and contractile stress, mechanical properties, and interfacial bonding. We also demonstrated individual and independent sensing and actuation with an array of LACs under different light projection patterns. The cephalopodinspired color modulation using a light-responsive material can potentially lead to a new concept for various engineering applications such as a camouflage interface, biophotonic device, and flexible display.

2. EXPERIMENTAL SECTION

2.1. Materials. Poly(ethylene glycol) diacrylate, $M_{\rm n} \sim 250$ (PEGDA 250), poly(ethylene glycol) diacrylate, $M_{\rm n} \sim 700$ (PEGDA 700), acrylic acid (AA), phenylbis(2,4,6-trimethylbenzoyl)-phosphine oxide (photoinitiator, PI), iron(III) nitrate nonahydrate, dopamine hydrochloride, and ammonium hydroxide solution were purchased from Sigma-Aldrich. *N*-Isopropylacrylamide (NIPAAm) was purchased from Fisher Scientific. All materials were used as received. Table 1 provides the chemicals and their concentrations in the precursor solutions used in each study.

2.2. Synthesis of Polydopamine Nanoparticles (PDA-NPs). PDA-NPs were synthesized via oxidation and a self-polymerization procedure. ¹⁶ Briefly, 2 mL of ammonium hydroxide solution (NH $_4$ OH) was mixed with 80 mL of ethanol and 180 mL of deionized water (DI water) and stirred at room temperature for 10 min. One gram of dopamine hydrochloride was dissolved in 20 mL of deionized water and then added into the above solution. The solution was stirred in the dark at room temperature for 30 h to allow dopamine polymerization. The PDA-NPs were then fully dried in a temperature oven (80 °C) overnight.

Table 1. Material Composition of Photocurable Precursor Solutions

	material composition					
study	monomer (M)	covalent cross-linker (PEGDA700) (M)	PI (mM)	PDA-NPs (g/L)	ionic cross-linker (Fe ³⁺ ion) (mM)	solvent
photoactive hydrogel (Section 3.1)	NIPAAm (2.6)	0.36	47.8	10 20 30		ethanol
cross-linker concentration study for AA hydrogel (Section 3.2)	AA (3.0)	0.02 0.05 0.10 0.20 0.40 0.80	47.8		15	ethanol
Fe ³⁺ concentration study for AA hydrogel (Section 3.2)	AA (3.0)	0.02	47.8		0 5 10 15 20 25 30	ethanol
mechanical properties for 3 materials (Section 3.3)	PEGDA250 NIPAAm	0.36	47.8	30		ethanol
	(2.6) AA (3.0)	0.02			15	ethanol

- **2.3. Photothermal Effect of PDA-NP Solution.** Seven solutions were prepared with predetermined PDA-NP concentrations (0, 0.31, 0.62, 1.25, 10, 20, and 30 g/L). The PDA-NPs were dispersed in DI water and stirred in the dark at room temperature overnight. 34 μ L of each solution was added into a transparent 96-well microplate (well diameter: 0.654 cm), resulting in the level of the solution being 1 mm from the bottom. A commercial digital projector (PJD6531w/DLP, ViewSonic) was used as a light source to trigger the photothermal effect. The intensity of the projected light on the surface of the solution was 0.77 W/cm² when a white image was projected. The temperature of the solutions was monitored using a thermocouple and recorded with LabVIEW.
- **2.4. Fabrication of Photoactive Hydrogel with PDA-NPs.** To prepare a photocurable precursor solution for a photoactive hydrogel, 2.6 M NIPAAm was dissolved in ethanol with 0.36 M of cross-linker (PEGDA 700) and 47.8 mM of PI. Then, PDA-NPs were added to the precursor solution as a photothermal agent. The solution was mixed in the dark at room temperature overnight. The photoactive hydrogel was then produced using a UV light source, UV oven, or custom-built MM-PµSL system.
- **2.5.** Fabrication of a Stretchable Acrylic Acid (AA) Hydrogel with Fe³⁺ lons. To prepare the photocurable precursor solution for a stretchable AA hydrogel, 3 M of AA was mixed with 47.8 mM of PI. Then, cross-linker (PEGDA 700) and iron(III) nitrate nonahydrate were added to the solution. The solution was mixed in the dark at room temperature overnight. The AA hydrogel was then produced using a UV light source, UV oven, or custom-built MM-PµSL system.
- 2.6. Sample Preparation for Swelling Ratio and Photothermal Effect Studies. A glass mold consisting of two microscope slides with 300 μ m-thick spacers is filled with the photocurable precursor solution. It was placed in a UV oven (CL-1000L, UVP, 365 nm) and cured with a light energy of 1320 mJ cm⁻², yielding a cross-linked hydrogel film. Then, samples in a disk shape were created from the film using a punch tool with a diameter of 4.8 mm. All samples were placed in DI water at room temperature overnight for rinsing.
- **2.7. Swelling Ratio Measurement.** The swelling ratio of the hydrogel samples was obtained by optically measuring the diameter of the disk samples. The samples were put into a temperature-controlled chamber filled with DI water. The chamber has a transparent glass window through which the temperature dependent deformation of samples was observed and measured. The temperature of water in the

- chamber was controlled within a range from 10 to 60 $^{\circ}$ C at a rate of 0.4 $^{\circ}$ C/min. The swelling ratio of the sample was measured at every 5 $^{\circ}$ C. Once the target temperature was reached, the temperature was kept constant for one hour, allowing the sample to reach equilibrium swelling. Then, a photo image of the sample was taken using a digital camera. The diameter of the sample was measured from the image using image analysis software, ImageJ.
- 2.8. Photothermally Triggered Temperature Change in a Photoactive Hydrogel. A commercial digital projector (PJD6531w/DLP, ViewSonic) was used as a light source (intensity of projected light: 0.77 W/cm²). Black-and-white image patterns were generated using a computer and projected on a photoactive hydrogel sample. The temperature of the hydrogel sample was monitored using a thermal camera (TIM 640, Microepsilon).
- **2.9.** Measurement of a Contractile Force of a Photoactive Hydrogel. To measure a contractile force of a photoactive hydrogel with increasing temperature, rectangular specimens (dimensions: 30 mm \times 5 mm \times 150 μ m; PDA-NP concentration: 30 g/L) were prepared using a glass mold and a UV oven. Then, dynamic mechanical analysis (DMA) was conducted on a dynamic mechanical analyzer (DMA 850, TA Instruments) with a submersion tension clamp. All samples were tested in iso-strain mode with temperature increasing from room temperature to 50 °C at a rate of 1 °C/min.
- **2.10. Mechanical Property Measurement.** To measure the mechanical properties of the three materials (photoactive hydrogel, stretchable AA hydrogel, and PEGDA 250), rectangular specimens (25 mm \times 4 mm \times 1 mm (or 300 μ m)) were prepared using a glass mold and a UV oven (light energy: 1320 mJ cm $^{-2}$). The cured samples were rinsed in DI water at room temperature overnight. Mechanical properties of the materials were measured on a dynamic mechanical analyzer (DMA 850, TA Instruments) using two clamps: a film tension clamp for AA samples and a submersion tension clamp for PNIPAAm and PEGDA samples. All samples were tested at room temperature with a strain rate of 0.33%/s and a preload force of 0.001 N.
- **2.11.** Interfacial Bonding Strength Measurement. To measure the interfacial bonding strength between two different materials, multimaterial rectangular specimens (30 mm \times 4 mm \times 300 μ m) were prepared using a glass mold and a UV oven. For a photoactive hydrogel/PEGDA interface, a rectangular photoactive hydrogel was fabricated first in a glass mold (15 mm \times 4 mm \times 300

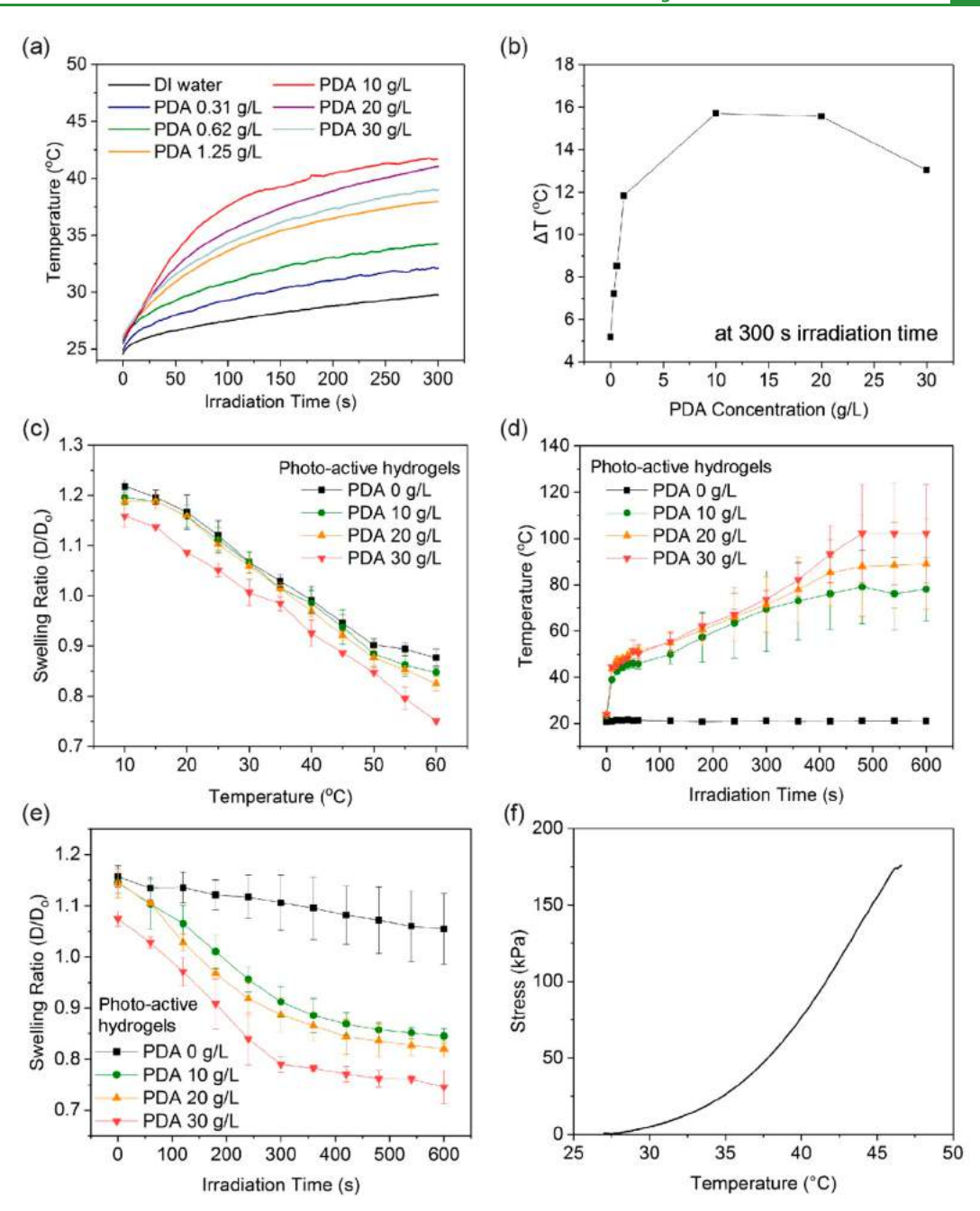


Figure 2. Light sensing muscle using photoactive hydrogel. (a) Effect of the PDA concentration on the temperature of the PDA solution under light irradiation. (b) Temperature increase in the PDA solutions at 300 s of light irradiation. (c) Swelling behavior of the photoactive hydrogels in response to temperature. (d) Photothermal heating of the photoactive hydrogels under light irradiation. (e) Light-induced shrinkage of the photoactive hydrogels. (f) Contractile stress of the photoactive hydrogel with 30 g/L PDA-NPs as temperature increases.

 μ m) using a UV oven (light energy: 1320 mJ cm⁻²). Then, the PEGDA precursor solution was injected into the space next to the cured photoactive hydrogel. The PEGDA solution was then cured using a UV oven (light energy: 1320 mJ cm⁻²). The samples were rinsed in DI water at room temperature overnight. For an AA hydrogel/photoactive hydrogel interface, the AA hydrogel was cured first in a glass mold, followed by curing a photoactive hydrogel next to it. The bonding strength between materials was measured on a dynamic mechanical analyzer (DMA 850, TA Instruments) using a film tension clamp. All samples were tested at room temperature with a strain rate of 0.33%/s and a preload force of 0.001 N.

2.12. Multimaterial Projection Microstereolithography (MM-PµSL). Multimaterial printing of the LAC with the three materials was achieved using MM-PµSL. The MM-PµSL system was built with the following major components: a UV LED (405 nm,

Innovations in Optics), a digital micromirror device (DMD) (extracted from a P1 projector, ASUS, Taipei, Taiwan), a projection lens (magnification of 0.2×, GCA Tropel, Fairport, NY), linear stages (Newport Corporation, Irvine, CA), a vacuum pump (Parker, Cleveland, OH), and 2-way pinch valves (Reet Corporation, Berlin, CT). All components of the system are controlled by a custom-written LabVIEW (National Instruments) script. The first material is supplied between a transparent window and a linear stage displaced by a predetermined distance (layer thickness). Then, patterned UV light is projected on the interface between the material and the window to photopolymerize the precursor solution. Next, the residual material in the printing area is removed with a vacuum pump, followed by an automatic sequence for cleaning with ethanol three times. Then, the next material is supplied to the printing area to

continue printing with the second material. This process is repeated until all three materials are printed to fabricate the LAC.

2.13. Postprinting Process. After 3D printing, the samples were rinsed and stored in DI water at room temperature overnight in order to rinse out the remaining uncross-linked polymers in the printed polymer network and achieve equilibrium swelling at room temperature. The typical volume of the DI water used for rinsing was 50 mL for each sample.

3. RESULTS AND DISCUSSION

3.1. Light Sensing Muscles Using Photoactive Hydrogel. As a material for a light-responsive muscle, we used a temperature-responsive hydrogel, poly(N-isopropylacrylamide) (PNIPAAm), with an embedded photothermal agent that converts light energy to heat. 17-26 PNIPAAm, one of the most widely used temperature-responsive hydrogels, exhibits a reversible volume change in water at its lower critical solution temperature (LCST, typically 32-35 °C). The PNIPAAm hydrogel swells at temperatures below the LCST and shrinks at temperatures above the LCST. 27-29 While embedded in the PNIPAAm hydrogel, photothermal agents generate heat upon light exposure, which subsequently raises the temperature of the hydrogel, leading to volume shrinkage of the hydrogel (Figure 1e). We used the PDA-NP as a photothermal agent because it has a high photothermal conversion efficiency, allowing for effective conversion of light energy into heat. Furthermore, its molecular structure containing both catechol and amine groups, similar to that of mussel-adhesive proteins, renders it highly adhesive to a wide range of materials. ^{23,30,31} Therefore, PNIPAAm with embedded PDA-NPs was selected as a light-responsive muscle of the LAC.

3.1.1. Photothermal Effect of PDA-NPs. The PDA-NPs were synthesized via oxidation and a self-polymerization procedure (see details in Experimental Section 2.2). 16 To study the photothermal effect of the PDA-NPs, PDA-NP solutions in deionized water (DI water) were prepared with varying concentrations, and their temperature change was monitored during light exposure. A commercial digital projector was used as a light source (intensity of projected light: 0.77 W/cm²), and the temperature of the solutions was measured using a thermocouple (see details in Experimental Section 2.3). As shown in Figure 2a, when the concentration of PDA-NPs falls within a range of 0-10 g/L, the solution temperature increased faster with increasing PDA-NP concentration, resulting in a higher solution temperature. Interestingly, the temperature increase was slower with higher concentrations of PDA-NAs (i.e., 20 and 30 g/L) (Figure 2b). We attribute this to the fact that the light penetration depth is significantly reduced with a high concentration of PDA-NPs (Figures S1 and S2; see details in the Supporting Information), resulting in less overall PDA-NPs in the solution receiving light energy to be converted to heat. Using a heating profile with light irradiation and a cooling profile without light as shown in Figure S3a, we calculated the photothermal conversion efficiency of the PDA-NPs (Figure S3; see details in the Supporting Information). 16 The obtained photothermal efficiency of the solution is ~25%, which is comparable and even higher than other previously reported photothermal agents, such as gold nanoparticles (3.4-9.9%), gold nanorods (17-22%), and semiconductor nanoparticles (27-30%).²⁵

3.1.2. Characterization of Photoactive Hydrogel. The key attribute of the photoactive hydrogel is its ability to create deformation in response to light via a photothermal effect of

the embedded PDA-NPs. To quantify light-responsive deformation, we use a lengthwise swelling ratio in this study, defined as a ratio of deformed length to the original length (as fabricated). For example, a swelling ratio is greater than 1 when the hydrogel swells and less than 1 when it shrinks. First, we studied the baseline swelling behavior of the photoactive hydrogel in response to temperature by monitoring its size in a temperature-controlled water chamber (Figure 2c). Diskshaped photoactive hydrogel samples with a diameter of 4.8 mm and a thickness of 300 μ m were fabricated (see details in Experimental Section 2.6). The NIPAAm and cross-linker (poly(ethylene glycol) diacrylate, $M_{\rm n} \sim 700$, PEGDA 700) concentrations in the photocurable precursor solution were 2.6 and 0.36 M in ethanol, respectively. Four samples were prepared with different PDA-NP concentrations: 0, 10, 20, and 30 g/L. As shown in Figure 2c, all samples showed a similar temperature-responsive swelling behavior: swelling at low temperature and shrinking at high temperature. While there was no significant effect of PDA-NP concentration on the swelling ratio of the hydrogel, we observed a slight decrease in the swelling ratio with increasing PDA-NPs over the entire test temperature range (10-60 °C). This is attributed to the fact that abundant catechol functional groups on the surface of the PDA-NPs form additional cross-linking in the hydrogels. 23,30,31

We also investigated photothermal heating of the photoactive hydrogel under light irradiation (Figure 2d). To study the effects of the PDA-NP concentration, four disk-shaped samples were prepared with different PDA-NP concentrations: 0, 10, 20, and 30 g/L. The samples were first allowed to swell in water and placed under projection light in air after water on the sample surface was removed. Then, the temperature of the sample was monitored with a thermal camera. All samples with PDA-NPs generated sufficient heat to increase the temperature of the hydrogel over the LCST, achieving their maximum temperature within 500 s (Figure 2d). The similar temperature increase among all three PDA-NP concentrations in the early stage of the experiment could be due to possible evaporative cooling on the sample surface. However, a higher PDA-NP concentration resulted in a higher temperature in general. On the other hand, no temperature change was observed in the pure PNIPAAm sample. This result confirms that the lightinduced heating was due to the photothermal effect of the embedded PDA-NPs.

Next, we studied light-induced deformation of the photoactive hydrogel. Four disk-shaped samples were prepared with different PDA-NP concentrations: 0, 10, 20, and 30 g/L. The samples were first allowed to swell in water and placed under projection light in air after water on the sample surface was removed. Then, diameters of the samples were measured at every 1 min to determine the swelling ratio. As shown in Figure 2e, the photoactive hydrogels showed light-induced shrinkage when they were exposed to light. All samples with PDA-NPs showed a similar shrinkage observed in the experiment conducted in a temperature-controlled water chamber (Figure 2c), confirming the effective photothermal heat generation by the embedded PDA-NPs. The higher PDA-NP concentration resulted in further shrinkage, which is consistent with the results shown in Figure 2c,d. The slight reduction in size of the PNIPAAm without PDA-NPs is attributed to moderate heating by possible light absorption to the PNIPAAm hydrogel itself and the test substrate on which the samples were placed. On the basis of the results, the photoactive hydrogel with 30 g/L PDA-NPs was chosen as the

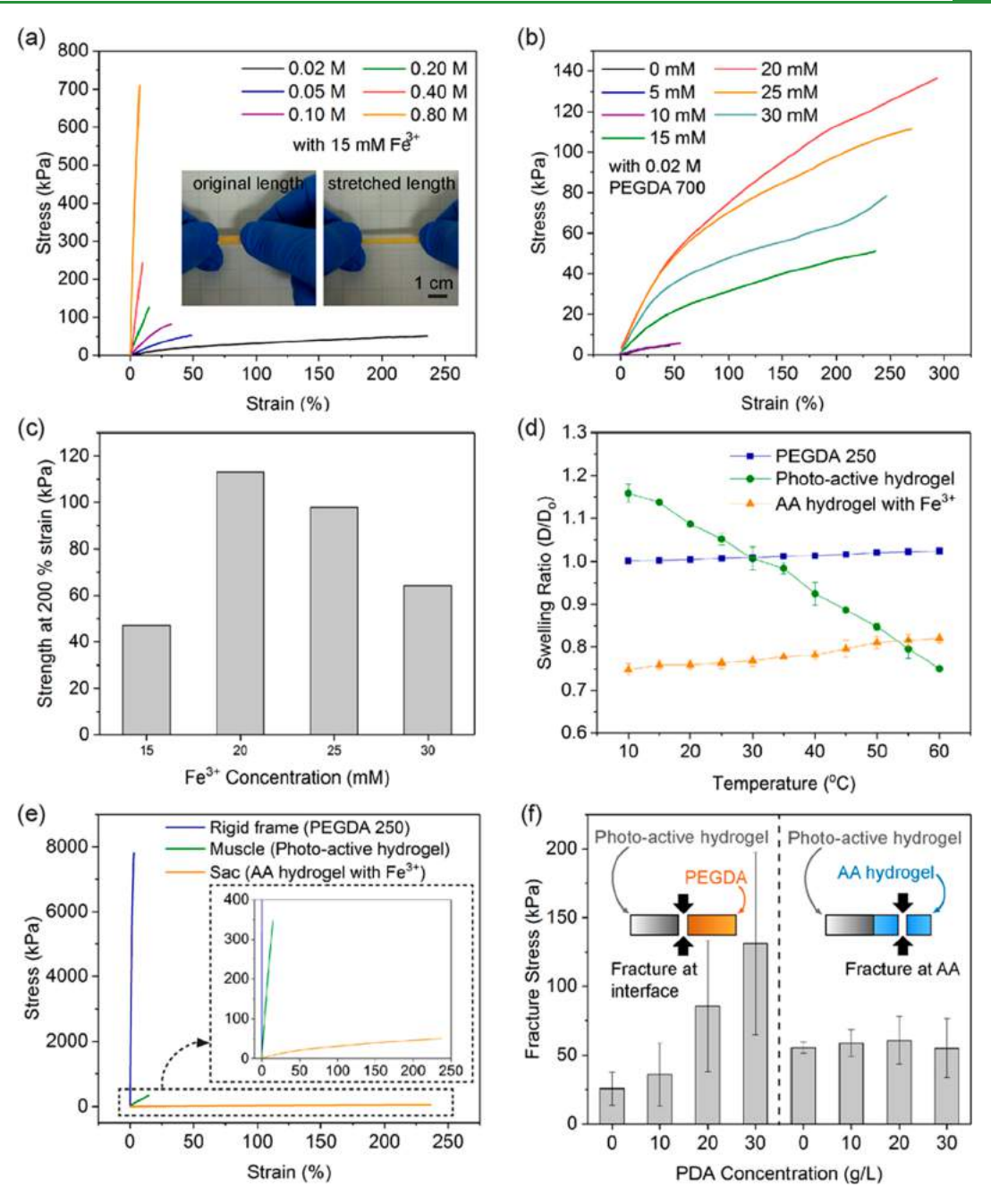


Figure 3. Mechanical property of LAC. (a) Effects of cross-linker (PEGDA 700) concentration on the mechanical properties of the acrylic acid (AA) hydrogels. The concentration of Fe³⁺ was fixed at 15 mM. (b) Improvement of mechanical properties by introducing Fe³⁺ ions to the AA hydrogel. The concentration of the cross-linker (PEGDA 700) was fixed at 0.02 M. (c) Stress required to stretch the AA hydrogels up to three times of their original length (strain of 200%). The AA hydrogel with 15 mM Fe³⁺ ions requires the lowest stress. (d) Swelling behavior of the three constituent materials of the LAC, PEGDA 250, the photoactive hydrogel, and the AA hydrogel over a temperature change. (e) Mechanical properties of the three constituent materials of the LAC. PEGDA 250 shows the high stiffness (~8 MPa). (f) Enhancing the interfacial bonding strength between different materials using PDA-NPs. Effect of the PDA-NP concentration on the bonding strength between the photoactive hydrogel and PEGDA 250 (left half) and between the photoactive hydrogel and the AA hydrogel (right half).

material for the light-responsive muscle. While it can create $\sim\!\!30\%$ reduction in length (or $\sim\!\!65\%$ reduction in volume) in response to light, it is the case for free shrinkage where there is no mechanical constraint. Since its contraction should be able to stretch the elastic sac, it is also important to characterize the stress it develops during shrinkage in order to design the artificial chromatophore. We prepared a rectangular photoactive hydrogel sample (30 mm \times 5 mm \times 150 μ m) with 30 g/L PDA-NPs and measured the stress generated as the temperature increased using DMA in the iso-strain mode

(i.e., the strain was forced to remain zero throughout the experiment). Figure 2f shows that contractile stress increased with temperature until it fractured. From the results from multiple experiments (n=4), the maximum contractile stress that the photoactive hydrogel can produce was determined to be 196.2 ± 28.5 kPa, which sets the upper bound of the stress required to stretch the artificial sac.

3.2. Stretchable Sac Using Acrylic Acid (AA) Hydrogel. In an actual chromatophore, the elastic sac can be stretched up to about three times in diameter. To achieve this

capability, it is necessary to create an artificial sac with a stretchable material. We employed a double-network (DN) approach to create a highly stretchable hydrogel for the sac of the LAC. DN hydrogels, typically consisting of two different polymer-chain networks (long- and short-chain networks), rely on the fracture of a short-chain network for energy dissipation and the interpenetration of a long-chain network for maintaining high elasticity, which significantly increases the toughness of the hydrogels. 32 In addition, the use of reversible physical cross-linking via hydrogen bonding,^{33–35} a lamellar bilayer, 36 or an ionic interaction 37 enables repeatable and reversible deformation (or stretching). For example, a large and recoverable deformation of acrylic acid (AA) hydrogel was demonstrated by involving Fe3+ ions. 38 Under deformation, the covalently cross-linked AA polymer chains remain intact to maintain their original configuration, while the reversible ionic cross-linking enabled by Fe3+ ions is broken to dissipate energy.

As the mechanical properties of the AA hydrogels are significantly influenced by the contents of covalent crosslinkers and ions, we studied the effects of covalent and ionic cross-linker concentrations on the mechanical properties of the AA hydrogel. First, the AA hydrogels prepared with different covalent cross-linker (PEGDA 700) contents were tested to study the effect of covalent cross-linker concentration on mechanical properties of the AA hydrogel. Six rectangular samples (25 mm \times 4 mm \times 1 mm) were prepared with different cross-linker concentrations, 0.02, 0.05, 0.10, 0.20, 0.40, and 0.80 M, in which the Fe³⁺ contents were fixed at 15 mM. Figure 3a shows the stress-strain curves of the 6 samples. When the concentration of the covalent cross-linker was increased, the elastic modulus of the hydrogel increased while the stretchability was reduced. Specifically, the AA hydrogels fabricated with 0.02 M of cross-linker can be stretched up to three times (200% strain) or more of its original length (insets of Figure 3a and Video S1).

We also studied the effect of Fe³⁺ ion concentration on the mechanical properties of the AA hydrogel. Seven rectangular AA hydrogel samples (25 mm × 4 mm × 1 mm) were fabricated with different Fe3+ ion contents: 0, 5, 10, 15, 20, 25, and 30 mM. The PEGDA 700 was fixed at 0.02 M. As shown in Figure 3b, the introduction of Fe³⁺ ions to the AA hydrogels improved the mechanical properties significantly. The pure AA hydrogel fabricated without Fe3+ showed much weaker mechanical properties, with a strength of 4.42 kPa and a failure strain of 45.4%. When Fe³⁺ ion content was less than 10 mM, the increase in mechanical properties was not prominent. However, with Fe³⁺ ions over 15 mM, the mechanical properties of the AA hydrogel were dramatically enhanced. In particular, with 20 mM of the Fe³⁺ ion concentration, the strength and failure strain were enhanced by more than 30 times (136.4 kPa) and 6 times (293.5%), respectively, compared to the pure AA hydrogel. A further increase in Fe³⁺ concentration, however, started to degrade the mechanical performance. This could be explained by the fact that Fe³⁺ ions have a negative influence on the free radical polymerization, resulting in lower and inhomogeneous cross-linking density. The Fe³⁺ ion concentration in the AA hydrogel for the sac was determined to be 15 mM because of its lowest required stress (47.1 kPa) at a strain of 200% (or 3 times of its original length). This is also lower than the maximum contractile stress that the photoactive hydrogel can produce, confirming that the sac can be effectively stretched up to three times through the

light-responsive contraction of the photoactive hydrogel (Figure 3c).

3.3. Mechanical Properties of Three Major Components for an Artificial Chromatophore. In addition to the photoactive hydrogel as a light-responsive muscle and the AA hydrogel as a stretchable sac, we also used PEGDA 250 as a rigid frame material because of its relatively stable swelling behavior over the temperature change (less than 3% increase in swelling ratio at 60 °C) (Figure 3d) and high mechanical stiffness (~8 MPa) (Figure 3e) compared to the other two materials. This also holds true over the range of operational temperatures of the LACs (Figure S6).

Although a large number of multimaterial 3D structures have been demonstrated with various multimaterial 3D printing techniques,³⁹ the weak bonding strength between different materials in the structure remains a critical problem in functional applications. PDA contains both catechol and amine groups in the structure, resulting in high adhesiveness to a wide range of materials. 23,30,31 PDA-NPs in our photoactive hydrogel also enhance the bonding strength with the other constituent materials of the LAC, PEGDA 250, and the AA hydrogel. As shown in the left half of Figure 3f, the higher the PDA-NP concentration in the photoactive hydrogel, the higher is the bonding strength between the photoactive hydrogel and PEGDA. With 30 g/L PDA-NPs, the bonding strength was 131 kPa, which was more than five times higher than that of the sample without PDA-NPs (25 kPa). It was also two times greater than the fracture strength (51 kPa) of the AA hydrogel with 15 mM Fe³⁺ ions (Figure 3c). It shows that the bonding strength between the photoactive hydrogel and PEGDA 250 is sufficient to survive the functioning of the LAC. Also, the bonding strength between the photoactive hydrogels and the AA hydrogel is shown in the right half of Figure 3f. Since the bonding strength between the two materials is higher than the fracture strength of the AA hydrogel, the fracture always occurred in the AA hydrogels without a separation at the interface regardless of the PDA-NP concentration. Although the exact bonding strength between the two materials was not determined, the result shows that the interfacial bonding is sufficiently large to operate the LAC. Our experiment also showed that the interfacial bonding at the material interfaces is not compromised at the elevated temperature of 60 °C, thereby allowing one to maintain the structural integrity of the multimaterial LAC throughout its actuation cycle (Figure S7).

3.4. Multimaterial Printing of an Artificial Chromatophore. We employed a multimaterial micro 3D printing technique to fabricate LACs using the three materials discussed above. Such an approach of 3D printing with shape shifting materials has been termed as 4D printing. 40-44 As discussed, the materials for photoactive muscle, stretchable sac, and rigid frame (Figure 1c) were the photoactive hydrogel with 30 g/L PDA-NPs, the AA hydrogel with 15 mM Fe3+ ions, and PEGDA 250, respectively. For processing different materials using MM-PµSL, the relationship between light energy for photopolymerization and curing depth was studied for all three materials to ensure printing consistency across different materials (Figure S4; see details in the Supporting Information). 12,45 On the basis of the results, multimaterial printing of the LAC with the three materials was achieved using MM-PµSL (see Table S1 for the printing process parameters). First, the rigid frame was printed with a length of 15 mm and a width of 4.5 mm. Then, two separated light-

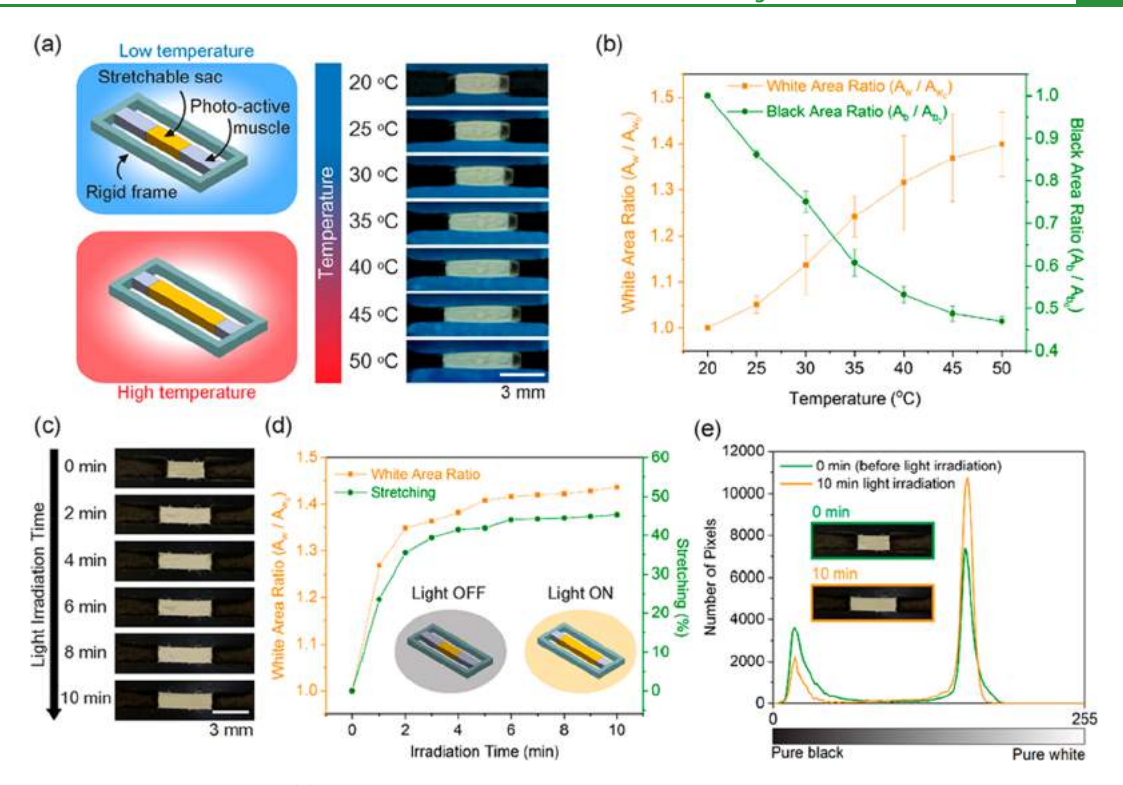


Figure 4. Printed LAC using MM-P μ SL. (a) Actuation of the LAC in response to temperature. Two light-responsive muscles contracted and stretched the artificial sac as the temperature increased. (b) Analysis of the associated color modulation of the LAC. White area ratio (orange squares) and black area ratio (green circles) are defined as a ratio of the area (A_w : white color area; A_b : black color area) to the original area (A_{w_0} : white color area; A_{b_0} : black color area). (c) Photo images of the LAC and its color modulation with light irradiation. (d) Change in the white area of the LAC with light exposure. (e) Histograms of the photo images of the LAC taken before and after light projection.

responsive muscles were created, a length of 3 mm and a width of 1.5 mm, integrating the muscles with the rigid frame. Finally, the stretchable sac was fabricated with the same dimension as the muscle filling the gap between the two separated muscles (Figure 1c). After printing, the LACs were stored in DI water at room temperature overnight for the postprinting process (see details in Experimental Section 2.13).

Since the base material for the photoactive hydrogel is a temperature-responsive hydrogel, PNIPAAm, the photoactive muscle can be activated by two different external stimuli, temperature and light. To characterize the baseline performance of the LAC, the shape change of the LAC was monitored in a water chamber while water temperature was varied within a range from 20 to 50 °C at a rate of 0.4 °C/min (Video S2). As shown in Figure 4a, as the temperature increased, two muscles (the photoactive hydrogel, black color) of the LAC contracted and stretched the sac (the AA hydrogel, white color). To analyze the associated color modulation of the LAC, two different color areas, black (muscles) and white (sac), of the LAC were measured and plotted in Figure 4b. While the temperature changed from 20 to 50 °C, the white color area (sac of the LAC) expanded by about 40% (orange square line in Figure 4b) and the black color area (muscles of the LAC) decreased by about 55% (green circle line in Figure 4b). This change is reversible and repeatable (see the Supporting Information and Figure S5). The large area changes for two different colors in response to temperature suggest that the LAC can effectively create an optical effect using the color modulation of the LAC.

We also demonstrated the color modulation of the LAC with light irradiation (Figure 4c). The LAC was placed

between two cover glasses with 100 µL of DI water. Then, white light (intensity of projected light: 0.77 W/cm²) was projected on the LAC using a commercial digital projector. Photo images of the LAC were taken every 1 min (total irradiation time: 10 min) using a digital camera. The photoactive muscles contracted and successfully stretched the sac up to about 40% (after 10 min) (Figure 4c and 4d). The white color area of the LAC was measured to analyze the color modulation of the LAC (Figure 4d). The graph shows that more than 95% of the total size change of the sac was achieved within only two minutes of light irradiation. The color modulation was also confirmed by the histograms of the photo images taken before and after light projection (Figure 4e). With the projection light, the signal of the dark colored pixels in the photo image was suppressed, while bright colored pixels increased. It indicates that the overall color tone of the LAC shifted from black to white upon light irradiation. In addition, actuation speed and the degree of modulation of the LAC are dependent on the intensity of light irradiation (Figure **S8**).

3.5. Cephalopod-Inspired Artificial Chromatophore Array. Cephalopods' camouflage is fundamentally different from that found in other animals and man-made devices in that each chromatophore detects light input and responds to alter the size of its sac by itself without centralized control, thereby collectively creating a variety of skin color patterns mimicking its surrounding environment. Inspired by this remarkable ability, we printed an array of three LACs with MM-P μ SL. ⁴⁶ The printed LAC array is shown in the inset in Figure 5. To demonstrate the distributed sensing and actuation, the LAC array was placed between two cover glasses with 300 μ L of DI

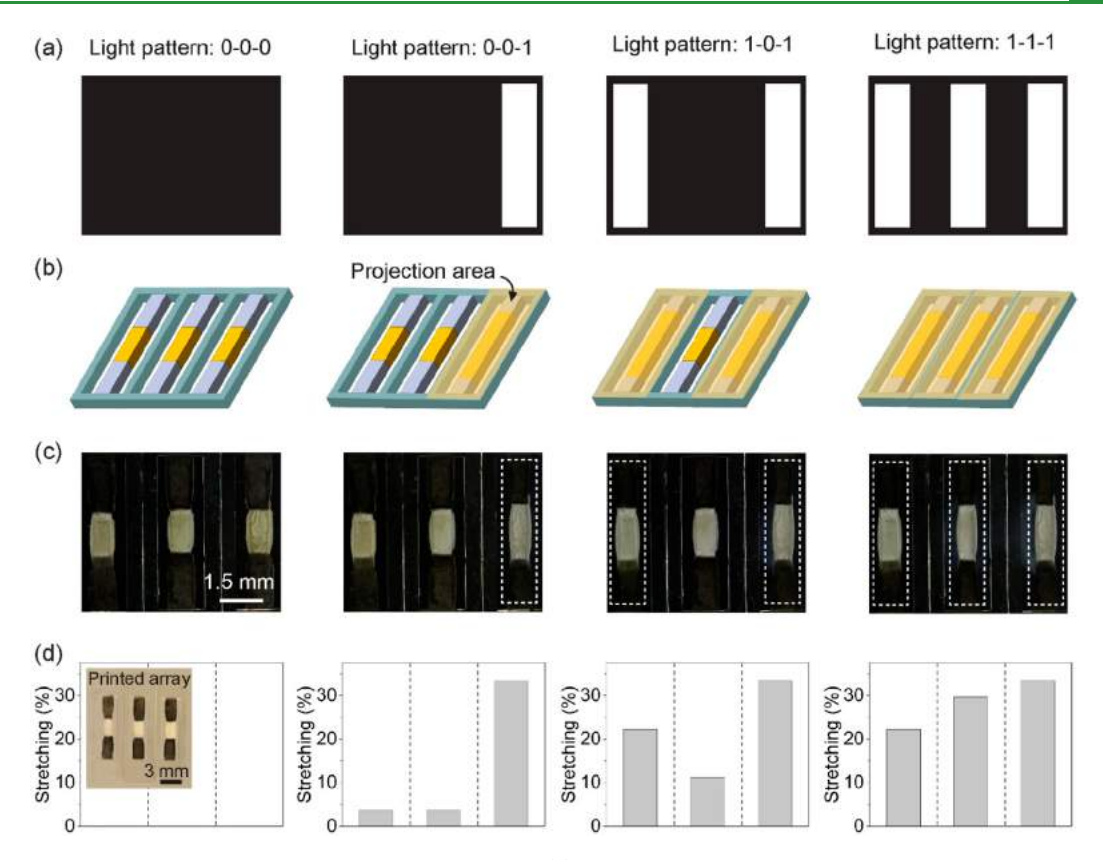


Figure 5. Printed LAC array and its distributed sensing and actuation. (a) Patterned black-and-white digital images used for light projection. (b) Schematics of the actuation of the LAC array under three different light projection patterns (0-0-1, 1-0-1, and 1-1-1). (c) Photo images of the LAC array after two minutes of exposure to the corresponding projection patterns. (d) Stretching of the sac in each LAC in the array according to light projection.

water and exposed to four different binary light patterns (0–0–0, 0–0–1, 1–0–1, and 1–1–1), where 0 and 1 indicate light-off and light-on, respectively, on the corresponding LAC unit (Figure 5). The order goes from left to right. As shown in Figure 5, only artificial chromatophore units with light exposure were fully stretched, suggesting that the color pattern of the LAC array can mimic the light projection pattern through light sensing and actuation of individual LAC units. Some cross-talking (unwanted stretching of a sac) was also observed in the LACs next to the light projection areas, because of heat transfer from the exposed LACs. An additional mechanism to thermally isolate each LAC unit would improve the performance for a more distinctive pattern generation.

4. CONCLUSIONS

We presented a multimaterial printed LAC that can sense light and modulate its color pattern at the individual unit level following the cephalopods' camouflage mechanism. Using a temperature-responsive hydrogel, PNIPAAm, with embedded PDA-NPs as a photothermal agent, we developed a photoactive hydrogel that can contract in response to light. We found that the photoactive hydrogel including 30 g/L PDA-NPs generated sufficient heat under light irradiation, resulting in a volume shrinkage up to 65% with a maximum contractile stress of 196 kPa. The stretchable sac was emulated by a double network AA hydrogel with Fe³⁺ ions, which showed a failure strain over 200%. We employed multimaterial $P\mu$ SL to integrate the two hydrogels along with PEGDA as a rigid frame to fabricate LACs in which a large area change of the AA

hydrogel was created by light-induced contraction of the photoactive hydrogel. The photothermal agent, PDA-NPs, also enhanced interfacial bonding strength between different materials by more than 5 times. The color tone of the LAC shifted from black to white within 2 min of light projection from a digital projector. We also demonstrated the creation of various binary color patterns from an LAC array (three LACs), mimicking the unique ability of the cephalopods' chromatophores to sense and actuate as an independent unit. While our study presents an artificial materials system that can turn light input into color patterns, addressing a few limitations can further improve its performance for practical application. First, the addition of different dyes to the AA hydrogel (sac) can change the current black-and-white binary color pattern to a more vibrant color expression. Also, various designs for the LAC unit can be explored to maximize its color fill factor (or minimize the inactive area not participating in color modulation). The reduction of heat transfer between LAC units would improve the performance for a more distinctive pattern generation. Despite these limitations, we believe that our LAC may suggest a new concept for various engineering applications such as a camouflage interface, biophotonic device, and flexible display.

ASSOCIATED CONTENT

Supporting Information

The Supporting Information is available free of charge at https://pubs.acs.org/doi/10.1021/acsami.0c17623.

Figures and discussion of the absorbance measurement of the PDA-NP solution, light penetration depth study for PDA solutions, calculation of the photothermal conversion efficiency of PDA-NPs, curing depth study for photocurable precursor solutions, repeatability and reversibility of LAC actuation, effect of temperature on mechanical properties of material components, interfacial bonding strength at high temperature, and effect of light intensity on the actuation of LAC; table of MM-P μ SL process parameters (PDF)

High stretchability of AA hydrogel (MP4) Color modulation of a printed LAC (MP4)

AUTHOR INFORMATION

Corresponding Author

Howon Lee — Department of Mechanical and Aerospace Engineering, Rutgers University, New Brunswick, New Jersey 08854, United States; ⊙ orcid.org/0000-0001-5778-2398; Email: howon.lee@rutgers.edu

Authors

Daehoon Han – Department of Mechanical and Aerospace Engineering, Rutgers University, New Brunswick, New Jersey 08854, United States; orcid.org/0000-0002-2526-3443

Yueping Wang – Department of Mechanical and Aerospace Engineering, Rutgers University, New Brunswick, New Jersey 08854, United States

Chen Yang — Department of Mechanical and Aerospace Engineering, Rutgers University, New Brunswick, New Jersey 08854, United States

Complete contact information is available at: https://pubs.acs.org/10.1021/acsami.0c17623

Author Contributions

[#]D.H. and Y.W. contributed equally.

Author Contributions

D.H. and H.L. conceived the concept and developed the design. D.H. and Y.W. performed all experiments with assistance from C.Y. All authors contributed to the data analysis and discussion. D.H. and H.L. wrote the manuscript. H.L. supervised the study.

Notes

The authors declare no competing financial interest.

ACKNOWLEDGMENTS

The authors gratefully acknowledge the financial support from Rutgers University Research Council Grant and the National Science Foundation (CBET-1804591 and CMMI-2001081).

REFERENCES

- (1) Fingerman, M. Chromatophores. *Physiol. Rev.* **1965**, 45, 296–339.
- (2) Bell, G. R.; Kuzirian, A. M.; Senft, S. L.; Mäthger, L. M.; Wardill, T. J.; Hanlon, R. T. Chromatophore Radial Muscle Fibers Anchor in Flexible Squid Skin. *Invertebr. Biol.* **2013**, *132*, 120–132.
- (3) Rossiter, J.; Yap, B.; Conn, A. Biomimetic Chromatophores for Camouflage and Soft Active Surfaces. *Bioinspiration Biomimetics* **2012**, 7, 036009.
- (4) Cloney, R. A.; Florey, E. Ultrastructure of Cephalopod Chromatophore Organs. *Cell Tissue Res.* **1968**, *89*, 250–280.
- (5) Mäthger, L. M.; Denton, E. J.; Marshall, N. J.; Hanlon, R. T. Mechanisms and Behavioural Functions of Structural Coloration in Cephalopods. *J. R. Soc., Interface* **2009**, *6*, S149–S163.

- (6) Kreit, E.; Mäthger, L. M.; Hanlon, R. T.; Dennis, P. B.; Naik, R. R.; Forsythe, E.; Heikenfeld, J. Biological Versus Electronic Adaptive Coloration: How Can One Inform the Other? *J. R. Soc., Interface* **2013**, *10*, 20120601.
- (7) Wang, Q.; Gossweiler, G. R.; Craig, S. L.; Zhao, X. Cephalopod-Inspired Design of Electro-Mechano-Chemically Responsive Elastomers for on-Demand Fluorescent Patterning. *Nat. Commun.* **2014**, 5, 4899.
- (8) Zeng, S.; Zhang, D.; Huang, W.; Wang, Z.; Freire, S. G.; Yu, X.; Smith, A. T.; Huang, E. Y.; Nguon, H.; Sun, L. Bio-Inspired Sensitive and Reversible Mechanochromisms Via Strain-Dependent Cracks and Folds. *Nat. Commun.* **2016**, *7*, 11802.
- (9) Yang, J.; Lee, H.; Heo, S. G.; Kang, S.; Lee, H.; Lee, C. H.; Yoon, H. Squid-Inspired Smart Window by Movement of Magnetic Nanoparticles in Asymmetric Confinement. *Adv. Mater. Technol.* **2019**, *4*, 1900140.
- (10) Xu, C.; Stiubianu, G. T.; Gorodetsky, A. A. Adaptive Infrared-Reflecting Systems Inspired by Cephalopods. *Science* **2018**, 359, 1495–1500.
- (11) Xu, C.; Colorado Escobar, M.; Gorodetsky, A. A. Stretchable Cephalopod-Inspired Multimodal Camouflage Systems. *Adv. Mater.* **2020**, 32, 1905717.
- (12) Han, D.; Yang, C.; Fang, N. X.; Lee, H. Rapid Multi-Material 3d Printing with Projection Micro-Stereolithography Using Dynamic Fluidic Control. *Addit. Manuf.* **2019**, *27*, 606–615.
- (13) Choi, J.-W.; MacDonald, E.; Wicker, R. Multi-Material Microstereolithography. *Int. J. Adv. Manuf.* **2010**, 49, 543–551.
- (14) Kowsari, K.; Akbari, S.; Wang, D.; Fang, N. X.; Ge, Q. High-Efficiency High-Resolution Multimaterial Fabrication for Digital Light Processing-Based Three-Dimensional Printing. 3D Print. Addit. Manuf. 2018, 5, 185–193.
- (15) Ge, Q.; Li, Z.; Wang, Z.; Zhang, W.; He, X.; Zhou, J.; Fang, N. Projection Micro Stereolithography Based 3d Printing and Its Applications. *Int. J. Extreme Manuf.* **2020**, *2*, 022004.
- (16) Liu, Y.; Ai, K.; Liu, J.; Deng, M.; He, Y.; Lu, L. Dopamine-Melanin Colloidal Nanospheres: An Efficient near-Infrared Photo-thermal Therapeutic Agent for in Vivo Cancer Therapy. *Adv. Mater.* **2013**, *25*, 1353–1359.
- (17) Jung, H. S.; Verwilst, P.; Sharma, A.; Shin, J.; Sessler, J. L.; Kim, J. S. Organic Molecule-Based Photothermal Agents: An Expanding Photothermal Therapy Universe. *Chem. Soc. Rev.* **2018**, *47*, 2280–2297.
- (18) Day, E. S.; Morton, J. G.; West, J. L. Nanoparticles for Thermal Cancer Therapy. *J. Biomech. Eng.* **2009**, *131*, 074001.
- (19) Gorelikov, I.; Field, L. M.; Kumacheva, E. Hybrid Microgels Photoresponsive in the near-Infrared Spectral Range. *J. Am. Chem. Soc.* **2004**, *126*, 15938–15939.
- (20) Li, W.; Wang, J.; Ren, J.; Qu, X. 3d Graphene Oxide-Polymer Hydrogel: Near-Infrared Light-Triggered Active Scaffold for Reversible Cell Capture and on-Demand Release. *Adv. Mater.* **2013**, *25*, 6737–6743.
- (21) Lee, E.; Lee, H.; Yoo, S. I.; Yoon, J. Photothermally Triggered Fast Responding Hydrogels Incorporating a Hydrophobic Moiety for Light-Controlled Microvalves. *ACS Appl. Mater. Interfaces* **2014**, *6*, 16949–16955.
- (22) Shi, K.; Liu, Z.; Wei, Y.-Y.; Wang, W.; Ju, X.-J.; Xie, R.; Chu, L.-Y. Near-Infrared Light-Responsive Poly (N-Isopropylacrylamide)/ Graphene Oxide Nanocomposite Hydrogels with Ultrahigh Tensibility. ACS Appl. Mater. Interfaces 2015, 7, 27289–27298.
- (23) Han, L.; Zhang, Y.; Lu, X.; Wang, K.; Wang, Z.; Zhang, H. Polydopamine Nanoparticles Modulating Stimuli-Responsive Pnipam Hydrogels with Cell/Tissue Adhesiveness. *ACS Appl. Mater. Interfaces* **2016**, *8*, 29088–29100.
- (24) Kim, D.; Lee, H. S.; Yoon, J. Highly Bendable Bilayer-Type Photo-Actuators Comprising of Reduced Graphene Oxide Dispersed in Hydrogels. *Sci. Rep.* **2016**, *6*, 20921.
- (25) Wu, Y.; Wang, K.; Huang, S.; Yang, C.; Wang, M. Near-Infrared Light-Responsive Semiconductor Polymer Composite Hydrogels:

- Spatial/Temporal-Controlled Release Via a Photothermal "Sponge' Effect. ACS Appl. Mater. Interfaces 2017, 9, 13602–13610.
- (26) Wang, Z. J.; Li, C. Y.; Zhao, X. Y.; Wu, Z. L.; Zheng, Q. Thermo-and Photo-Responsive Composite Hydrogels with Programmed Deformations. *J. Mater. Chem. B* **2019**, *7*, 1674–1678.
- (27) Wu, C.; Wang, X. Globule-to-Coil Transition of a Single Homopolymer Chain in Solution. *Phys. Rev. Lett.* **1998**, *80*, 4092.
- (28) Zhang, X.-Z.; Xu, X.-D.; Cheng, S.-X.; Zhuo, R.-X. Strategies to Improve the Response Rate of Thermosensitive Pnipaam Hydrogels. *Soft Matter* **2008**, *4*, 385–391.
- (29) Han, D.; Lu, Z.; Chester, S. A.; Lee, H. Micro 3d Printing of a Temperature-Responsive Hydrogel Using Projection Micro-Stereo-lithography. *Sci. Rep.* **2018**, *8*, 1963.
- (30) Ding, Y.; Floren, M.; Tan, W. Mussel-Inspired Polydopamine for Bio-Surface Functionalization. *Biosurf. Biotribol.* **2016**, *2*, 121–136.
- (31) Kord Forooshani, P.; Lee, B. P. Recent Approaches in Designing Bioadhesive Materials Inspired by Mussel Adhesive Protein. J. Polym. Sci., Part A: Polym. Chem. 2017, 55, 9–33.
- (32) Zhao, X. Multi-Scale Multi-Mechanism Design of Tough Hydrogels: Building Dissipation into Stretchy Networks. *Soft Matter* **2014**, *10*, 672–687.
- (33) Nakajima, T.; Takedomi, N.; Kurokawa, T.; Furukawa, H.; Gong, J. P. A Facile Method for Synthesizing Free-Shaped and Tough Double Network Hydrogels Using Physically Crosslinked Poly (Vinyl Alcohol) as an Internal Mold. *Polym. Chem.* **2010**, *1*, 693–697.
- (34) Saito, J.; Furukawa, H.; Kurokawa, T.; Kuwabara, R.; Kuroda, S.; Hu, J.; Tanaka, Y.; Gong, J. P.; Kitamura, N.; Yasuda, K. Robust Bonding and One-Step Facile Synthesis of Tough Hydrogels with Desirable Shape by Virtue of the Double Network Structure. *Polym. Chem.* **2011**, *2*, 575–580.
- (35) Chen, Q.; Zhu, L.; Zhao, C.; Wang, Q.; Zheng, J. A Robust, One-Pot Synthesis of Highly Mechanical and Recoverable Double Network Hydrogels Using Thermoreversible Sol-Gel Polysaccharide. *Adv. Mater.* **2013**, *25*, 4171–4176.
- (36) Haque, M. A.; Kurokawa, T.; Kamita, G.; Gong, J. P. Lamellar Bilayers as Reversible Sacrificial Bonds to Toughen Hydrogel: Hysteresis, Self-Recovery, Fatigue Resistance, and Crack Blunting. *Macromolecules* **2011**, *44*, 8916–8924.
- (37) Sun, J.-Y.; Zhao, X.; Illeperuma, W. R.; Chaudhuri, O.; Oh, K. H.; Mooney, D. J.; Vlassak, J. J.; Suo, Z. Highly Stretchable and Tough Hydrogels. *Nature* **2012**, *489*, 133–136.
- (38) Zhong, M.; Liu, Y.-T.; Liu, X.-Y.; Shi, F.-K.; Zhang, L.-Q.; Zhu, M.-F.; Xie, X.-M. Dually Cross-Linked Single Network Poly (Acrylic Acid) Hydrogels with Superior Mechanical Properties and Water Absorbency. *Soft Matter* **2016**, *12*, 5420–5428.
- (39) Han, D.; Lee, H. Recent Advances in Multi-Material Additive Manufacturing: Methods and Applications. *Curr. Opin. Chem. Eng.* **2020**, 28, 158–166.
- (40) Tibbits, S. 4d Printing: Multi-Material Shape Change. Arch. Des. 2014, 84, 116–121.
- (41) Gladman, A. S.; Matsumoto, E. A.; Nuzzo, R. G.; Mahadevan, L.; Lewis, J. A. Biomimetic 4d Printing. *Nat. Mater.* **2016**, *15*, 413–418.
- (42) Yang, C.; Boorugu, M.; Dopp, A.; Ren, J.; Martin, R.; Han, D.; Choi, W.; Lee, H. 4d Printing Reconfigurable, Deployable and Mechanically Tunable Metamaterials. *Mater. Horiz.* **2019**, *6*, 1244–1250.
- (43) Han, D.; Morde, R. S.; Mariani, S.; La Mattina, A. A.; Vignali, E.; Yang, C.; Barillaro, G.; Lee, H. 4d Printing of a Bioinspired Microneedle Array with Backward-Facing Barbs for Enhanced Tissue Adhesion. *Adv. Funct. Mater.* **2020**, *30*, 1909197.
- (44) Yang, C.; Luo, J.; Polunas, M.; Bosnjak, N.; Chueng, S. T. D.; Chadwick, M.; Sabaawy, H. E.; Chester, S. A.; Lee, K. B.; Lee, H. 4d-Printed Transformable Tube Array for High-Throughput 3d Cell Culture and Histology. *Adv. Mater.* **2020**, *32*, 2004285.
- (45) Kim, N.; Bhalerao, I.; Han, D.; Yang, C.; Lee, H. Improving Surface Roughness of Additively Manufactured Parts Using a Photopolymerization Model and Multi-Objective Particle Swarm Optimization. *Appl. Sci.* **2019**, *9*, 151.

(46) Zheng, X.; Deotte, J.; Alonso, M. P.; Farquar, G. R.; Weisgraber, T. H.; Gemberling, S.; Lee, H.; Fang, N.; Spadaccini, C. M. Design and Optimization of a Light-Emitting Diode Projection Micro-Stereolithography Three-Dimensional Manufacturing System. *Rev. Sci. Instrum.* **2012**, *83*, 125001.